

Article

Alkaline Phosphatase-Triggered in Situ Formation of Silicon-Containing Nanoparticles for Fluorometric and Colorimetric Dual Channel Immunoassay

Chuanxia Chen, Dan Zhao, Bo Wang, Pengjuan Ni, Yuanyuan Jiang, Chenghui Zhang, Fan Yang, Yizhong Lu, and Jian Sun

Anal. Chem., **Just Accepted Manuscript** • DOI: 10.1021/acs.analchem.0c00224 • Publication Date (Web): 24 Feb 2020

Downloaded from pubs.acs.org on February 27, 2020

Just Accepted

“Just Accepted” manuscripts have been peer-reviewed and accepted for publication. They are posted online prior to technical editing, formatting for publication and author proofing. The American Chemical Society provides “Just Accepted” as a service to the research community to expedite the dissemination of scientific material as soon as possible after acceptance. “Just Accepted” manuscripts appear in full in PDF format accompanied by an HTML abstract. “Just Accepted” manuscripts have been fully peer reviewed, but should not be considered the official version of record. They are citable by the Digital Object Identifier (DOI®). “Just Accepted” is an optional service offered to authors. Therefore, the “Just Accepted” Web site may not include all articles that will be published in the journal. After a manuscript is technically edited and formatted, it will be removed from the “Just Accepted” Web site and published as an ASAP article. Note that technical editing may introduce minor changes to the manuscript text and/or graphics which could affect content, and all legal disclaimers and ethical guidelines that apply to the journal pertain. ACS cannot be held responsible for errors or consequences arising from the use of information contained in these “Just Accepted” manuscripts.

Alkaline Phosphatase-Triggered in Situ Formation of Silicon-Containing Nanoparticles for Fluorometric and Colorimetric Dual Channel Immunoassay

Chuanxia Chen,[†] Dan Zhao,^{‡,§} Bo Wang,[†] Pengjuan Ni,[†] Yuanyuan Jiang,[†] Chenghui Zhang,[†] Fan Yang,[‡] Yizhong Lu,^{*,†} and Jian Sun^{*,‡}

[†]School of Materials Science and Engineering, University of Jinan, Jinan, Shandong 250022, China

[‡]State Key Laboratory of Electroanalytical Chemistry, Changchun Institute of Applied Chemistry, Chinese Academy of Sciences, Changchun, Jilin 130022, China

[§]School of Environmental Engineering and Chemistry, Luoyang Institute of Science and Technology, Luoyang, Henan 471023, China

ABSTRACT: Enzyme-triggered in situ chromogenic and/or fluorogenic reactions under accessible conditions are significant for developing enzyme activity and related spectroscopic assays. Here, we describe a facile one-pot synthetic strategy to prepare silicon-containing nanoparticles (Si CNPs) with yellow-green fluorescence and orange-red color by mixing N-[3-(trimethoxysilyl)propyl]ethylenediamine and *p*-aminophenol (AP) in aqueous solution at a mild temperature. Encouraged by the AP-regulated simple synthetic procedure and the generation of AP from alkaline phosphatase (ALP)-catalyzed hydrolysis of 4-aminophenol phosphate (APP), a fluorometric and colorimetric dual-readout ALP activity assay can be rationally envisioned and developed by employing APP as the substrate. In the wake of the good analytical performance of such ALP activity assay and its successful combination with enzyme-linked immunosorbent assay (ELISA), corresponding fluorometric and colorimetric dual-readout ALP-based ELISA has been constructed for highly sensitive and quantitative determination of human prostate specific antigen (PSA), the key biomarker of prostate cancer in human serum. The convincing performance in evaluating PSA level in serologic test unambiguously reveals the great potential of our proposed fluorometric and colorimetric dual channel immunoassay in early clinic diagnosis by monitoring disease biomarkers.

Alkaline phosphatase (ALP), an enzyme that can catalyze the dephosphorylation of various phosphorylated species, is a significant biomarker for medical diagnostics. Abnormal activity of ALP in human serum is closely associated with many diseases, such as bone diseases, hepatobiliary diseases, chronic nephritis, and diabetes.¹ Moreover, due to its high turnover number, good stability, mild reaction conditions, and broad substrate specificity, ALP has been extensively used as a labeling enzyme in enzyme-linked immunosorbent assay (ELISA).² The highly specific antigen-antibody recognition and efficient biocatalytic properties of labeling enzymes endow ELISA with excellent specificity and high throughput,^{3,4} which boost ELISA as a powerful technique in clinical diagnosis and laboratory research.⁴⁻⁶

Because of the significance of ALP detection in disease diagnosis and extra establishment of ELISA platforms, many analytical methods such as colorimetry,⁶⁻⁹ fluorometry,¹⁰⁻¹⁶ surface enhancement Raman scattering,¹⁷ and electrochemistry have been developed to monitor ALP activity.^{18,19} Correspondingly, ALP-based colorimetric, fluorometric, and electrochemical immunoassays have been also reported.^{6,13-16,19} Among these strategies, colorimetric and fluorometric assays have highlighted for their simplicity in operation, cost effectiveness, and real-time monitoring capability. However, most of such routine optical ALP activity assays directly estimate the color or fluorescence variations between the

specially designed substrates and enzymatic hydrolysates,^{12,20} which suffer from poor sensitivity and laborious synthesis/purification procedures. Alternatively, nanomaterial-based ALP assays can often significantly improve the detection sensitivity and performances, profiting from the higher extinction coefficient and superior fluorescence properties of nanomaterials than small molecule probes.^{13,21-26} More particularly, the whole analysis procedures of immunoassays will be greatly simplified if the signal generation relies on in situ formed nanoprobe instead of the one prepared in advance. In addition, despite many advances in the fields of nanomaterial-based ALP assays and ALP-based ELISA, however, almost all of them focused on only single readout signal. It makes them susceptible to biological environment and operating conditions, which is not beneficial for achieving reliable, precise, and highly sensitive bioassays. Thus, it is still highly desirable to develop straightforward and highly sensitive multi-channel optical ALP assays, especially those based on the enzyme-enabled in situ generation of nanomaterials.

In recent years, silicon nanoparticles (Si NPs) have sparked wide research interests owing to their superior optical properties and good biocompatibility. Despite of the exciting progresses in preparing Si NPs, rapid synthetic strategies under accessible mild conditions are still urgently needed.²⁷ It has been already reported that Si NPs can be formed by

reducing silanes in a one-step reduction process.²⁸⁻³¹ However, the available reductants (typically ascorbic acid, hydroquinone, glucose or gramineae plants) are very limited, meanwhile, most synthetic processes need a long reaction time (e.g. 2 days) and/or high reaction temperature. What is more, to the best of our knowledge, almost all reports overlooked the intrinsic colorimetric properties of Si NPs and their potential application in dual readout optical assays. More significantly, the latest paper suggested that some silicon-containing nanomaterials are in fact not zero-valent silicon (Si⁰) NPs.³² Considering some previous reports indeed also indicated the absence of Si⁰,^{30,33,34} the nanomaterials synthesized in this work are temporarily termed as silicon-containing nanoparticles (Si CNPs).

4-aminophenol phosphate (APP) is a typical ALP substrate that can be transformed into *p*-aminophenol (AP) through the dephosphorylation reaction. Based on AP-triggered deposition of silver shells on different gold nanostructures (such as NPs, nanorods, and nanobipyramids), several APP-based colorimetric ALP activity assays and immunoassays have been reported.³⁵⁻³⁷ However, direct optical ALP assays with APP as the substrate, especially the fluorometric and colorimetric dual mode ones, are still in their infancy due to the lack of AP-participant chromogenic or fluorescent reactions.⁹ Herein, we first present an aqueous strategy for facile, one-step synthesis of Si CNPs, using AP and N-[3-(trimethoxysilyl)propyl]ethylenediamine (DAMO) as the precursors. The reaction can be completed within 20 min and the obtained Si CNPs with fluorometric and colorimetric dual signals are water dispersible, strongly photo-, salt- and pH-stable. Furthermore, the convenient and simple synthetic process of Si CNPs can achieve fluorometric and colorimetric ALP activity assays, inhibitor screening and ALP-based ELISAs based on the ALP-catalyzed generation of AP, AP-triggered in situ growth of Si CNPs and common ALP-labeled immunoassay. By taking human prostate specific antigen (PSA) as model antigen target, the proposed ELISA with good serologic test results may enable a diagnosis of prostate cancer.

EXPERIMENTAL SECTION

Chemicals and Materials. DAMO and AP were obtained from Aladdin Co. Ltd. (Shanghai, China). APP, ALP (EC 3.1.3.1) from bovine intestinal mucosa, PSA, α -fetoprotein (AFP), bovine serum albumin (BSA), lysozyme, glucose oxidase (GOx), and trypsin were purchased from Sigma-Aldrich (St. Louis, MO). Pancreatin, pepsin, and sodium vanadate (Na₃VO₄) were bought from Macklin Biochemical Technology Co. Ltd. (Shanghai, China). Mouse monoclonal anti-PSA antibody, rabbit polyclonal anti-PSA antibody, and ALP-conjugated secondary antibody were bought from Abcam (Cambridge, MA). Both the wash buffer and antibody dilution buffer for ELISA were purchased from Boster (Wuhan, China). Human serum samples from two normal adults were kindly supplied by the hospital of the University of Jinan.

Apparatus and Characterization. UV-vis spectra were recorded by a UV-8000 spectrophotometer (Metash, China). Fluorescence spectra were acquired with a Shimadzu RF-6000 spectrofluorometer (Shimadzu, Japan). The morphology of Si CNPs was characterized by using a Jeol JEM-2100 Plus transmission electron microscope (TEM, Japan) operated at 100 kV. X-ray photoelectron spectroscopy (XPS) study was

carried out using the ESCALAB MK II spectrometer (VG Scientific) with Al K α radiation as X-ray source. X-ray powder diffraction (XRD) pattern was collected on D8 ADVANCE (Germany) using Cu K α radiation generated at 40 kV and 40 mA. Fourier transform infrared (FTIR) data were acquired with a VERTEX 70 Fourier transform infrared spectrometer (Bruker).

Synthesis and Purification of Si CNPs. Typically, 1.6 mL of DAMO and 0.6 mL of AP solution (10 mM) were successively added into 7.8 mL of ultrapure water. The mixture was then incubated at 70 °C for 20 min in a water bath, during which the colorless solution gradually turned orange-red. The resulted Si CNPs were cooled to room temperature, purified with a dialysis bag (500 Da) against ultrapure water for 12 h, and then stored at 4 °C for further use.

Detection of ALP Activity. Typically, 100 μ L of APP (2 mM), 20 μ L of MgCl₂ (1 mM), 100 μ L of ALP with various activities and 540 μ L of ultrapure water were subsequently added into 200 μ L of Tris-HCl buffer (50 mM, pH 9.8), followed by incubation at 37 °C for 70 min. Afterward, 40 μ L of DAMO was added into the above reaction solution, and the absorbance and fluorescence intensities of resultant solutions were recorded directly after being incubated at 70 °C for 20 min.

Immunoassay for PSA. First, 96-well polystyrene plate was coated with mouse anti-PSA antibody (100 μ L, 5 μ g/mL) in coating solution at 4°C overnight. After discarding the solutions, the wells were washed three times with wash buffer (200 μ L), and then blocked with BSA (1%) at room temperature for 1 h. Subsequently, the plate was washed three times with wash buffer (200 μ L), and 100 μ L of PSA standard solutions (0–80 ng/mL) were added into each well. After 2 h at room temperature and the washing steps, rabbit anti-PSA antibody (100 μ L, 2 μ g/mL) was added for 2 h at room temperature. The plate was then washed three times, and ALP-conjugated secondary antibody (100 μ L, 1:3000) was added for 1 h at room temperature, followed by washing steps.

Afterward, the enzymatic reaction was performed as follows: 25 μ L of APP (2 mM), 5 μ L of MgCl₂ (1 mM) and 50 μ L of Tris-HCl buffer (50 mM, pH 9.8) were subsequently added into each well containing 160 μ L of ultrapure water, and then incubated at 37°C for 70 min. Afterward, 10 μ L of DAMO was introduced. The absorbance and fluorescence intensities of resultant solutions were recorded after being incubated at 70 °C for 20 min.

Immunoassay for the Real Clinical Samples. The detailed procedures of the dual-readout ELISA referred to those for the model protein by just adding the diluted human serums instead of the PSA standard solution.

RESULT AND DISCUSSIONS

Synthesis and Characterization of Si CNPs. DAMO, a silane containing two amine groups in each molecule, can react with some reductants such as catechol, hydroquinone, citrate, and EDTA to generate N-doped Si CNPs with the assistance of high temperature and pressure or microwave radiations.^{33,34,38,39} In this work, we proposed a more convenient and gentle synthetic protocol for DAMO-evolved Si CNPs with the assistance of AP for the first time (Figure 1A). As depicted in Figure S1, the incubation of DAMO with AP leads to the generation of an orange-red colored product,

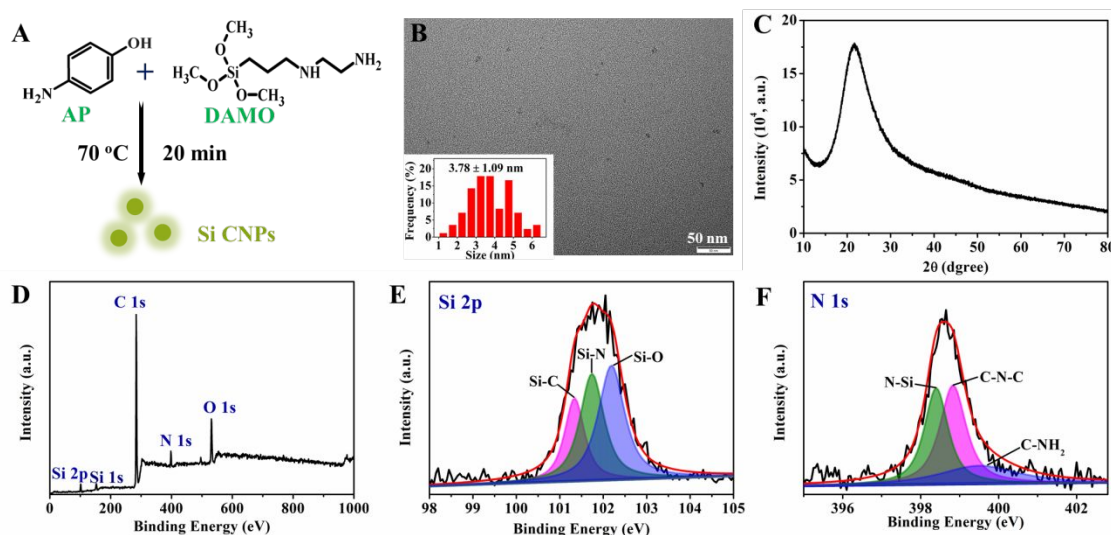


Figure 1. (A) Schematic illustration of one-pot synthesis of Si CNPs. (B) TEM, (C) XRD, and (D) XPS images of Si CNPs. Deconvoluted spectra of (E) Si 2p and (F) N 1s. The inset in B is the distribution histogram of particle size.

which emits distinct yellow-green fluorescence under the irradiation of UV light (365 nm), explicitly revealing that the formed Si CNPs possess both colorimetric and fluorescent properties. Control experiments show that DAMO alone or AP alone fails to provoke such chromogenic and fluorescent reactions (Figure S1). To obtain Si CNPs with the best fluorescence performances, the temperature and reaction time are optimized to be 70 °C and 20 min, respectively (Figure S2).

TEM image shows that the obtained Si CNPs present uniform particulate morphologies with an average diameter of 3.78 ± 1.09 nm (Figure 1B). The wide peak in XRD pattern indicates their roughly amorphous nature without any specific orientation (Figure 1C). Additionally, the element composition and surface of Si CNPs were analyzed by XPS and FTIR. As illustrated in Figure 1D, the five peaks at 284.50, 398.55, 531.85, 102.50, and 153.00 eV correspond to C 1s, N 1s, O 1s, Si 2p, and Si 1s. The three fitted peaks at 101.34, 101.74, and 102.19 eV in the Si 2p spectrum are assigned to Si-C, Si-N, and Si-O groups, respectively (Figure 1E). Consistent with the deconvoluted spectra of Si 2p, a sharp stretching vibration signal of Si-O at 1043 cm^{-1} can be observed in the FTIR spectrum (Figure S4). The deconvoluted spectra of C 1s display four signals for C-Si (284.00 eV), C-C/C=C (284.48 eV), C-N (285 eV), and C-OH/C-O-C (288.47 eV), respectively (Figure S3A). Peaks belonging to C=O (531.42 eV), C-OH/C-O-C (531.91 eV), and Si-O (533.29 eV) units can be observed in the deconvoluted spectra of O 1s (Figure S3B). The deconvoluted spectra of N 1s reveal the presence of N-Si (398.40 eV), C-N-N (398.83 eV), and C-NH₂ (399.50 eV) units (Figure 1F). FTIR spectrum further confirms the presence of abundant hydrophilic groups on the surface of Si CNPs, mainly -OH and -NH₂ groups, which endow Si CNPs with good aqueous dispersibility and stability. In addition, the presence of nitrogen element can effectively modulate the surface state and photic properties of the nanomaterials, finally facilitating better luminescent properties.³⁸

The optical properties of generated Si CNPs were analyzed in detail. The UV-vis spectrum of Si CNPs in Figure 2A displays several typical absorption peaks centered at approximately 376, 450, 480, and 510 nm. It is generally accepted that the peak at 376 nm, originated from the trapping

surface state, results in strong emission,⁴⁰ and the peaks at 450, 480, and 510 nm that may be assigned to the surface state transitions produce weak or nearly no observed fluorescence signal.⁴¹ Unsurprisingly, the maximum excitation peak is centered at 376 nm, and under the excitation of 376 nm, a symmetrical fluorescence emission peak centered at 524 nm can be observed. The quantum yield (QY) of Si CNPs excited with 376 nm is calculated to be 8.2% in reference to quinine sulfate (QY=54%, Figure S5). Significantly, as shown in Figure S6, the emission wavelength of Si CNPs does not shift when the excitation wavelength increases from 320 nm to 430 nm, demonstrating an excitation-independent emission behavior in a wide wavelength range. Conversely, when exciting under the wavelength of 440-480 nm, obvious red shift for the emission band can be observed and the fluorescence intensity decreases significantly. The excitation-independent and -dependent emission behaviors of Si CNPs could be attributed to the direct band gap transition and the oxygen induced defects, respectively.²⁹ For the subsequent application of Si CNPs in biosensing, we interrogated the stability of prepared Si CNPs and robust stability will be conducive to their potential biological applications. After 60 min of UV irradiation (376 nm, 150 W), the fluorescence of Si CNPs preserves about 94% of the initial intensity (Figure S7A), implying a remarkable photostability. Moreover, the fluorescence of Si CNPs is insensitive to ionic strength (Figure S7B). Notably, aqueous solution of Si CNPs maintains strong fluorescence in the wide pH range of 2.0–12.0 (Figure S7C and D). Such robust pH stability may be attributed to the plentiful surface-covered -OH/-NH₂ groups, which can serve as protective shells around the nanoparticles.

In view of the fact that the indispensable reagent for Si CNPs generation (i.e., AP) can be in situ produced from the ALP-catalyzed dephosphorylation of APP, the present synthetic process has the potential to achieve ALP activity assay. First, the relationship between optical signals of resultant Si CNPs and AP concentrations was evaluated. As depicted in Figure 2B-E, both the absorbance and fluorescence intensity of the DAMO-AP solution progressively grow stronger with the increased concentrations of AP, accompanied with the gradual color change from colorless to orange-red under daylight and yellow-green under the UV

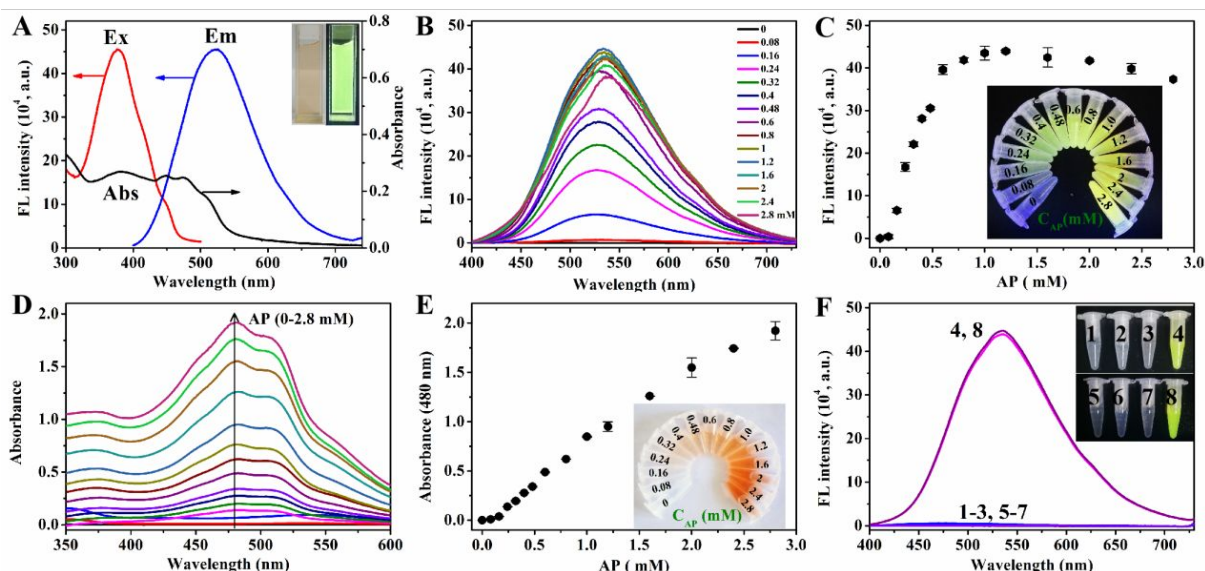


Figure 2. (A) UV-vis absorption and fluorescent spectra of Si CNPs. Insets are the photographs of Si CNP solution under daylight and under 365 nm UV light. (B) Fluorescence and (D) UV-vis absorption spectra of Si CNPs with different concentrations of AP. (C) Fluorescence intensity and (E) absorbance of DAMO toward AP with various concentrations. Insets are the corresponding photographs. (F) Fluorescence spectra of the resulted solutions of control (1, 5), DAMO (2, 6), AP (3, 7), and DAMO + AP (4, 8) without (1-4) and with Tris-HCl (pH 9.8, 10 mM, 5-8). The inset shows the corresponding solutions under 365 nm UV light.

irradiation. The AP concentration-dependent optical signals of Si CNPs provide a possibility for the subsequent quantitation of ALP activity. As is well-known, ALP triggered dephosphorylation reaction can only work well under alkaline conditions, especially in a strong alkaline condition of pH 9.8. Fortunately, Tris-HCl buffer with a pH value of pH 9.8 never hamper the generation of Si CNPs (Figure 2F). Consequently, the fluorometric and colorimetric dual-readout assay for ALP activity based on AP-triggered synthesis of Si CNPs can be developed and utilized in the Tris-HCl buffer (pH 9.8).

Fluorometric and Colorimetric Dual-Readout Assays of ALP Activity. The sensing principle is depicted in Figure 3A. ALP catalyzes the hydrolysis of APP to generate AP, the generated AP then reacts DAMO to produce Si CNPs. The feasibility of this ALP assay was then studied by UV-vis and fluorescence spectra. When ALP-treated APP is introduced into the DAMO solution, intense colorimetric and fluorescent signals can be observed (d, Figure 3B and C). In striking contrast, the solutions of DAMO, DAMO-ALP, and DAMO-APP are unable to emit discernible fluorescence (b and c, Figure 3B) and produce unique absorption peaks of Si CNPs (b and c, Figure 3C). These results imply that DAMO is sensitive only to the ALP-catalyzed dephosphorylation of APP, validating the possibility of ALP detection based on the excellent ability of DAMO to distinguish APP and AP.

To guarantee a preferable analytical performance for this ALP activity assay, experimental conditions including substrate (APP) and activator ($MgCl_2$) concentrations, enzymatic reaction time, and DAMO concentration have been optimized. Since the detection range and sensitivity of an enzyme assay are directly related to the substrate concentration, APP concentration is evaluated first and optimized to be 0.2 mM (Figure S8A). It has been reported that Mg^{2+} with a suitable concentration can effectively activate the ALP activity and increase its stability against autolysis.¹³ As expected, Mg^{2+} substantially enhances the activity of ALP (Figure S8B) without blocking the formation of Si CNPs (Figure S9). Based on the results in Figure S8B, 20 μM Mg^{2+}

is adopted in the following experiments because further increasing the Mg^{2+} concentration is unable to further enhance the fluorescence intensities. Additionally, the enzymatic reaction can be completed within 70 min, which is selected as the optimal reaction time (Figure S8C). After ascertaining the conditions for ALP-catalyzed hydrolysis of APP, different volumes of liquid DAMO are added to produce fluorescent Si CNPs. The fluorescence intensities increase gradually and then level off when the DAMO volume exceeds 40 μL (Figure S8D). Therefore, 40 μL DAMO is used in the following assay experiments.

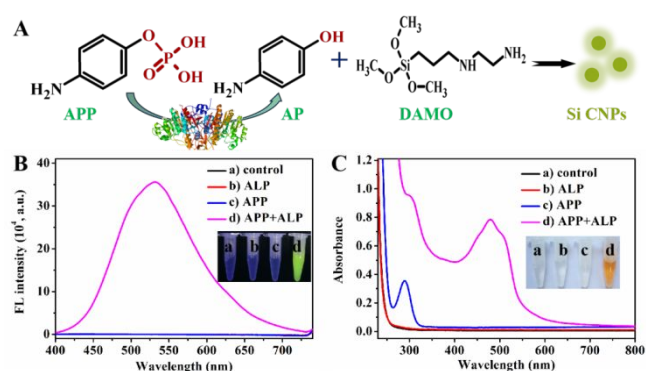


Figure 3. (A) Schematic representation of the ALP-triggered generation of Si CNPs with APP as the substrate. (B) Fluorescence and (C) UV-vis absorption spectra of the resulted solutions by adding water (black line), ALP (red line), APP (blue line), and APP + ALP (purple line) into DAMO. The insets in B and C show the corresponding solutions under 365 nm UV light and natural light, respectively.

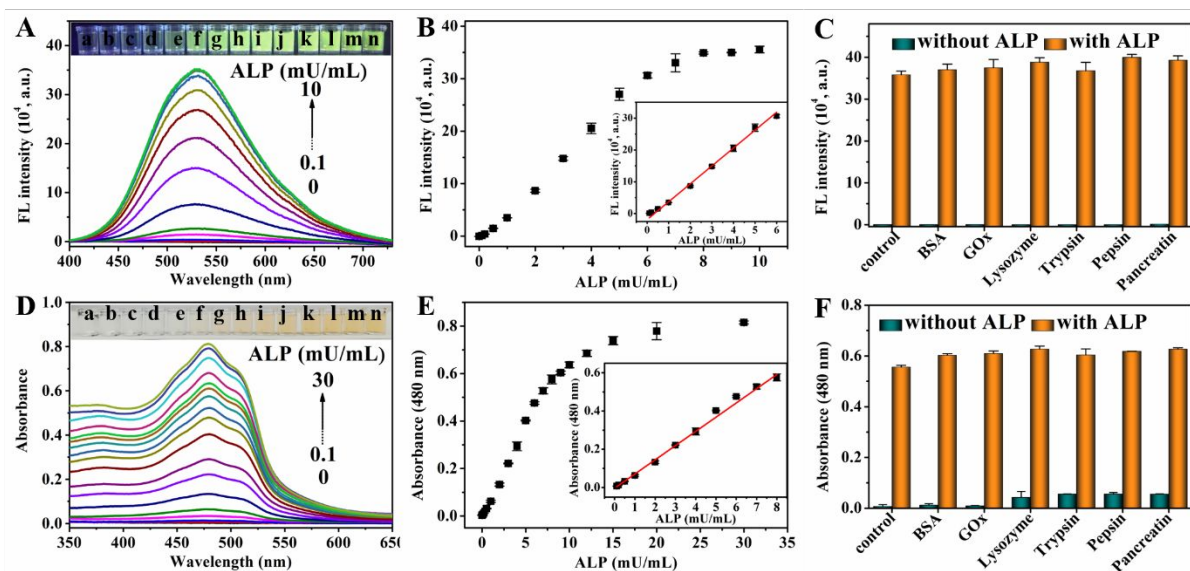


Figure 4. (A) Fluorescence and (D) UV-vis absorption spectra of the sensing system with different ALP activities (a-n: 0, 0.1, 0.2, 0.5, 1, 2, 3, 4, 5, 6, 7, 8, 9, 10 mU/mL). (B) Fluorescence intensities at 524 nm and (E) absorbance values at 480 nm versus various ALP activities. (C) Fluorescence and (F) colorimetric responses of the proposed system against control enzymes/proteins (10 $\mu\text{g/mL}$) in the absence and presence of ALP (6 mU/mL). Inserts in A and D are the corresponding photographs under 365 nm UV light and natural light, respectively.

Under the optimal conditions, the sensing ability of this fluorometric and colorimetric dual-readout ALP activity assay were assessed. As shown in Figure 4, both fluorescent signal and colorimetric signal exhibit an ALP activity-dependent enhancement behavior, and the obvious color changes can be easily distinguished with naked eyes (inserts in Figure 4A and D). With the increased activity of ALP, gradual increases of fluorescence intensity and absorbance are observed (Figure 4A and D) due to the increased concentration of in situ produced AP through the gradual hydrolysis of APP. Figure 4B manifests that the fluorescence intensity centered at 524 nm (F_{524}) has a good linear relationship with the ALP activities in the range of 0.1–6.0 mU/mL. The fitted linear equation can be expressed as $F_{524} = 56250 C_{\text{ALP}} (\text{mU/mL}) - 18845$, $R^2 = 0.989$. Compared to the fluorometric assay, the colorimetric one exhibits a wider linear range (0.1–8.0 mU/mL). The linear fitting equation between the absorbance at 480 nm (A_{480}) and ALP activities can be expressed as $A_{480} = 0.074 C_{\text{ALP}} (\text{mU/mL}) - 0.003$, $R^2 = 0.992$ (Figure 4E). The detection limits for fluorometric and colorimetric readout modes are correspondingly calculated to be 0.0022 mU/mL and 0.011 mU/mL ($3\sigma/S$). Notably, when ALP activity exceeds 0.5 mU/mL (d, Figure 4A) and 2.0 mU/mL (f, Figure 4D), the fluorometric and colorimetric colors are visually distinguishable from the original ones. These results suggest that our dual-readout assay displays excellent analytical performance in ALP detection compared to other ALP assays (Table S1), providing a vital precondition for its extensive bioassay applications and the establishment of high-efficient dual-mode immunoassay.

To investigate the specificity of the proposed ALP assay, we challenged it with several common proteins and enzymes, including BSA, GOx, lysozyme, trypsin, pepsin, and pancreatin (10 $\mu\text{g/mL}$). None of them can evoke distinct changes in fluorescent intensity and absorbance of the sensing system (Figure 4C and F). The satisfactory selectivity can be ascribed to the highly specific hydrolysis of APP triggered by

ALP and will facilitate the ALP determination in biological samples.

Inhibitor Screening for ALP. Investigation on the inhibitor of enzyme is of great importance in drug design. Therefore, the proposed fluorometric and colorimetric dual-readout ALP assay has been further explored to evaluate the enzyme inhibition efficiency by using Na_3VO_4 , a well-acknowledged ALP inhibitor, as a model. The control experiments have ascertained that the addition of Na_3VO_4 alone is unable to affect the synthesis reaction of Si CNPs (Figure S10). Then, ALP is pretreated with different concentrations of Na_3VO_4 before being subjected to the substrate solution. With the addition of Na_3VO_4 , the release of AP (i.e., hydrolysis of APP) is restricted due to the effectual inhibition of ALP activity, and the formation of Si CNPs would be depressed ultimately. Accordingly, both the fluorescence intensity

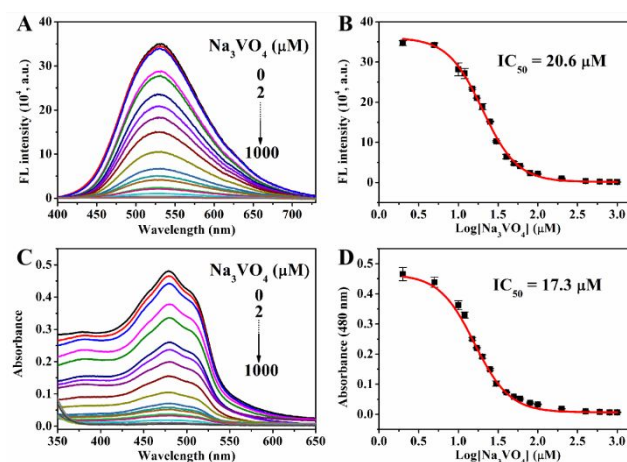


Figure 5. (A) Fluorescence and (C) UV-vis absorption spectra of the ALP assay with different concentrations of Na_3VO_4 . Sigmoidal fitting of the (B) fluorescence intensity and (D) absorbance versus the logarithm of Na_3VO_4 concentrations.

and absorbance decrease progressively with the increase of Na_3VO_4 concentrations from 0 to 1000 μM (Figure 5). Typical sigmoidal curves can be achieved when plotting the fluorescence intensity and absorbance versus the logarithm of the Na_3VO_4 concentrations. The IC_{50} (the inhibitor concentration required for 50% inhibition of the enzyme activity) values for fluorometric and colorimetric detections are calculated to be approximately 20.6 and 17.3 μM , respectively, which are in good accord with the reported values in other works.^{9,42} The above results clearly manifested that our method is prospective for the screening of ALP inhibitors.

Dual-Readout ELISA Strategy for PSA Detection.

Stimulated by the extensive and successful application of ALP in ELISA, we finally extended this fluorometric and colorimetric dual light-on ALP activity assay into a dual-readout ALP-labeled immunoassay. In this regard, PSA is chosen as the model antigen because it has been regarded as the key biomarker of prostate cancer.⁴³ The simple, accurate and sensitive detection of PSA is vital for the early prostate cancer treatment and may improve the survival rates of patients. The establishment of this dual-readout ELISA for the detection of PSA follows the procedures of conventional ELISA: capture antibody (capture ab), PSA standard with a series of concentrations, primary antibody (ab1), and ALP-secondary antibody conjugate (ALP-ab2) are successively immobilized on a 96-well plate via specific antigen-antibody immunoreactions. Then, APP is added to produce AP, and DAMO is subsequently injected to generate Si CNPs, providing fluorometric and colorimetric readout signals (Figure 6A). Both signals display PSA-dependent enhancement behaviors. The more PSA is introduced, the more ALP labeled on antibody would be banded. Correspondingly, the fluorescence intensity at 524 nm and the absorbance at 480 nm gradually increase when the PSA concentrations increase from 0 to 80 ng/mL (Figure 6B and D), exhibiting good linearity with PSA concentrations from 0.02 to 20 ng/mL and from 0.02 to 28 ng/mL (Figure 6C and E). The fluorometric linear equation can be described as $F_{524} = 313147 C_{\text{PSA}} (\text{ng/mL}) + 802$, $R^2 = 0.993$, and the colorimetric linear equation can be described as $A_{480} = 0.020 C_{\text{PSA}} (\text{ng/mL}) + 0.008$, $R^2 = 0.991$. The detection limit is 0.0041 and 0.0096 ng/mL calculated from $3\sigma/S$ for fluorometric and colorimetric detections. Such detection performance of our dual-readout assay is comparable or superior to that of most reported PSA assays (Table S2).

Furthermore, to investigate the selectivity toward PSA detection, the ELISA platform is challenged with other nonspecific proteins (AFP, BSA, lysozyme, and trypsin). Unsurprisingly, no distinct changes in fluorescence and colorimetric signals are observed for interfering proteins (Figure S11), manifesting that our dual readout ELISA can specifically recognize and quantitate target PSA in complicated matrix.

Encouraged by the splendid sensitivity and selectivity of this dual readout ELISA for PSA, we try to apply it to the detection of target PSA in real samples. For this purpose, two unrelated 50-fold diluted human serums containing different levels of PSA are analyzed. As revealed in Table S3, results obtained from this dual modal ELISA are well consistent with the results from the pNPP-based standard ELISA method, which verifies that our assay has a high accuracy and excellent performance in real sample analysis.

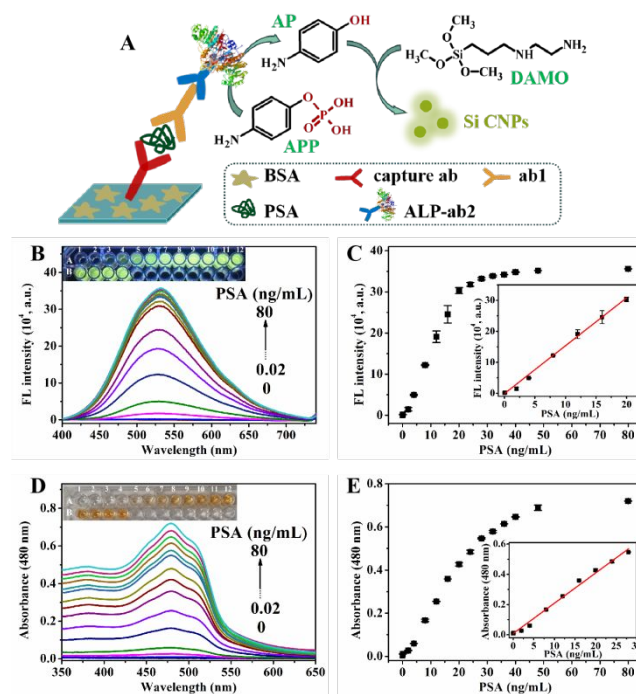


Figure 6. (A) Schematic representation of the dual-mode ELISA based on in situ generation of Si CNPs triggered by ALP. (B) Fluorescence and (D) UV-vis absorption spectra of the ELISA platform with different ALP activities. (C) Fluorescence intensities and (E) absorbance values versus various PSA concentrations. Inserts in B and D are the corresponding photographs under 365 nm UV light and natural light.

CONCLUSION

In summary, Si CNPs that possess both fluorometric and colorimetric signals have been synthesized by a facile, rapid, one-step approach using AP and DASO as the precursors for the first time. The prepared Si CNPs feature uniform morphology, good photophysical properties, and excellent aqueous dispersibility. Moreover, the fluorescent intensity and colorimetric signal of generated Si CNPs are related to the concentration of AP, inspired by which and the fact that AP can be in situ generated through ALP-catalyzed dephosphorylation of APP, a dual-readout ALP activity assay is thus anticipated by employing the in situ formation of Si CNPs as a signal generator. This ALP activity assay is further employed to establish a fluorometric and colorimetric dual channel light-on ELISA platform for PSA detection harnessing the conventional ALP-labeled immunoassay. The simultaneous but independent dual-signal quantification method can significantly improve the detection precision and diversity, reducing the false-positive and -negative rates in serodiagnosis. We believe our proposed analytical technique with facile sensing process and convincing dual-readout mode will possess high practicality and superiority in both laboratory research and clinical diagnosis in the near future.

ASSOCIATED CONTENT

Supporting Information

The Supporting Information is available free of charge on the ACS Publications website.

Fluorescent and UV-vis absorption spectra of AP, DAMO, and AP+DAMO; optimization of synthesis conditions; high resolution

C 1s and O 1s spectra, FTIR spectrum, and quantum yield of Si CNPs; fluorescent emission of Si CNPs at various excitation wavelength; stability of Si CNPs; optimization of experimental conditions for ALP detection; effect of MgCl₂ on the formation of Si CNPs; comparison of various ALP assays; effect of Na₃VO₄ on the formation of Si CNPs; comparison of various optical PSA assays; selectivity investigation of this ELISA; results of PSA detection in human serums (PDF).

AUTHOR INFORMATION

Corresponding Author

*E-mail: mse_luyz@ujn.edu.cn

*E-mail: jiansun@ciac.ac.cn; Fax: +86 431 85689278

Author Contributions

The manuscript was written through contributions of all authors.

Notes

The authors declare no competing financial interest.

ACKNOWLEDGMENT

This work was supported by the National Natural Science Foundation of China (21904048, 21705056, 21902062, and 21902061), the Young Taishan Scholars Program (tsqn201812080), the Natural Science Foundation of Shandong Province (ZR2018BB057 and ZR2019YQ10), the Doctoral Fund of University of Jinan (160100410) and the Youth Innovation Promotion Association, CAS (no. 2018258).

REFERENCES

- (1) Fernandez, N. J.; Kidney, B. A. *Vet. Clin. Pathol.* **2007**, *36*, 223-233
- (2) Aragay, G.; Pino, F.; Merkoci, A. *Chem. Rev.* **2012**, *112*, 5317-5338
- (3) Rissin, D. M.; Kan, C. W.; Campbell, T. G.; Howes, S. C.; Fournier, D. R.; Song, L.; Piech, T.; Patel, P. P.; Chang, L.; Rivnak, A. J.; Ferrell, E. P.; Randall, J. D.; Provuncher, G. K.; Walt, D. R.; Duffy, D. C. *Nat. Biotechnol.* **2010**, *28*, 595-599
- (4) Liang, J.; Yao, C.; Li, X.; Wu, Z.; Huang, C.; Fu, Q.; Lan, C.; Cao, D.; Tang, Y. *Biosens. Bioelectron.* **2015**, *69*, 128-134
- (5) de la Rica, R.; Stevens, M. M. *Nat. Nanotechnol.* **2012**, *7*, 821-824
- (6) Xianyu, Y. L.; Wang, Z.; Jiang, X. Y. *ACS Nano* **2014**, *8*, 12741-12747
- (7) Wei, H.; Chen, C. G.; Han, B. Y.; Wang, E. *Anal. Chem.* **2008**, *80*, 7051-7055
- (8) Zhao, W.; Chiuman, W.; Lam, J. C.; Brook, M. A.; Li, Y. *Chem. Commun.* **2007**, 3729-3731
- (9) Sun, J.; Zhao, J.; Bao, X. F.; Wang, Q. F.; Yang, X. R. *Anal. Chem.* **2018**, *90*, 6339-6345
- (10) Ma, J. L.; Yin, B. C.; Wu, X.; Ye, B. C. *Anal. Chem.* **2016**, *88*, 9219-9225
- (11) Kim, T. I.; Kim, H.; Choi, Y.; Kim, Y. *Chem. Commun.* **2011**, *47*, 9825-9827
- (12) Chen, C. X.; Yuan, Q.; Ni, P. J.; Jiang, Y. Y.; Zhao, Z. L.; Lu, Y. Z. *Analyst* **2018**, *143*, 3821-3828
- (13) Sun, J.; Hu, T.; Chen, C. X.; Zhao, D.; Yang, F.; Yang, X. R. *Anal. Chem.* **2016**, *88*, 9789-9795
- (14) Zhao, D.; Li, J.; Peng, C. Y.; Zhu, S. Y.; Sun, J.; Yang, X. R. *Anal. Chem.* **2019**, *91*, 2978-2984
- (15) Malashikhina, N.; Garai-Ibabe, G.; Pavlov, V. *Anal. Chem.* **2013**, *85*, 6866-6870
- (16) Chen, C. X.; Zhao, J. H.; Lu, Y. Z.; Sun, J.; Yang, X. R. *Anal. Chem.* **2018**, *90*, 3505-3511
- (17) Ruan, C. M.; Wang, W.; Gu, B. H. *Anal. Chem.* **2006**, *78*, 3379-3384
- (18) Goggins, S.; Naz, C.; Marsh, B. J.; Frost, C. G. *Chem. Commun.* **2015**, *51*, 561-564

- (19) Kreuzer, M. P.; O'Sullivan, C. K.; Guilbault, G. G. *Anal. Chim. Acta* **1999**, *393*, 95-102
- (20) Hou, X.; Yu, Q.; Zeng, F.; Ye, J.; Wu, S. *J. Mater. Chem. B* **2015**, *3*, 1042-1048
- (21) Deng, J.; Yu, P.; Wang, Y.; Mao, L. *Anal. Chem.* **2015**, *87*, 3080-3086
- (22) de la Rica, R.; Stevens, M. M. *Nat. Nanotechnol.* **2012**, *7*, 821-824
- (23) Xuan, Z. H.; Li, M. M.; Rong, P. F.; Wang, W.; Li, Y. J.; Liu, D. B. *Nanoscale* **2016**, *8*, 17271-17277
- (24) Chen, C. X.; Zhang, G. L.; Ni, P. J.; Jiang, Y. Y.; Lu, Y. Z.; Lu, Z. L. *Microchim Acta* **2019**, *186*, 348
- (25) Halawa, M. I.; Gao, W.; Saqib, M.; Kitte, S. A.; Wu, F.; Xu, G. *Biosens. Bioelectron.* **2017**, *95*, 8-14
- (26) Chen, C. X.; Zhao, D.; Jiang, Y. Y.; Ni, P. J.; Zhang, C. H.; Wang, B.; Yang, F.; Lu, Y. Z.; Sun, J. *Anal. Chem.* **2019**, *91*, 15017-15024
- (27) Song, B.; He, Y. *Nano Today* **2019**, *26*, 149-163
- (28) Sharma, B.; Tanwar, S.; Sen, T. *ACS Sustainable Chem. Eng.* **2019**, *7*, 3309-3318
- (29) Tiwari, A.; Sherpa, Y. L.; Pathak, A. P.; Singh, L. S.; Gupta, A.; Tripathi, A. *Mater. Today Commun.* **2019**, *19*, 62-67
- (30) Nsanamahoro, S.; Mutuyimana, F. P.; Han, Y.; Ma, S.; Na, M.; Liu, J.; Ma, Y.; Ren, C.; Chen, H.; Chen, X. *Sens. Actuators, B* **2019**, *281*, 849-856
- (31) Wang, J.; Ye, D.-X.; Liang, G.-H.; Chang, J.; Kong, J.-L.; Chen, J.-Y. *J. Mater. Chem. B* **2014**, *2*, 4338-4345
- (32) Oliinyk, B. V.; Korytko, D.; Lysenko, V.; Alekseev, S. *Chem. Mater.* **2019**, *31*, 7167-7172
- (33) Geng, X.; Li, Z.; Hu, Y.; Liu, H.; Sun, Y.; Meng, H.; Wang, Y.; Qu, L.; Lin, Y. *ACS Appl. Mater. Interfaces* **2018**, *10*, 27979-27986
- (34) Han, Y.; Chen, Y.; Feng, J.; Liu, J.; Ma, S.; Chen, X. *Anal. Chem.* **2017**, *89*, 3001-3008
- (35) Zhou, C.-H.; Zhao, J.-Y.; Pang, D.-W.; Zhang, Z.-L. *Anal. Chem.* **2014**, *86*, 2752-2759
- (36) Yang, X.; Gao, Z. *Chem. Commun.* **2015**, *51*, 6928-6931
- (37) Xu, S.; Ouyang, W.; Xie, P.; Lin, Y.; Qin, B.; Lin, Z.; Chen, G.; Guo, L. *Anal. Chem.* **2017**, *89*, 1617-1623
- (38) Wu, F.-G.; Zhang, X.; Kai, S.; Zhang, M.; Wang, H.-Y.; Myers, J. N.; Weng, Y.; Liu, P.; Gu, N.; Chen, Z. *Adv. Mater. Interfaces* **2015**, *2*
- (39) Liu, Y.; Wang, Q.; Guo, S.; Jia, P.; Shui, Y.; Yao, S.; Huang, C.; Zhang, M.; Wang, L. *Sens. Actuators, B* **2018**, *275*, 415-421
- (40) Dong, Y.; Pang, H.; Yang, H. B.; Guo, C.; Shao, J.; Chi, Y.; Li, C. M.; Yu, T. *Angew. Chem. Int. Edit.* **2013**, *52*, 7800-7804
- (41) Zhu, S.; Shao, J.; Song, Y.; Zhao, X.; Du, J.; Wang, L.; Wang, H.; Zhang, K.; Zhang, J.; Yang, B. *Nanoscale* **2015**, *7*, 7927-7933
- (42) Zhao, J.; Wang, S.; Lu, S.; Bao, X.; Sun, J.; Yang, X. *Anal. Chem.* **2018**, *90*, 7754-7760
- (43) Lilja, H.; Ulmert, D.; Vickers, A. J. *Nat. Rev. Cancer* **2008**, *8*, 268-278

for TOC only

